







New Parameters for Star Cluster Dynamics: The Effect of Primordial Binaries and Dark Remnants

B. Bhat^{1,2} , B. Lanzoni^{1,2} , F. R. Ferraro^{1,2} , and E. Vesperini³ ¹ Dept. of Physics and Astronomy “A. Righi,” University of Bologna, Via Gobetti 93/2, Bologna, Italy; bhvana.pb.bhat@gmail.com² INAF Osservatorio di Astrofisica e Scienza dello Spazio di Bologna, Via Gobetti 93/3, Bologna, Italy³ Dept. of Astronomy, Indiana University, Bloomington, IN 47401, USA

Received 2022 September 5; revised 2023 January 16; accepted 2023 January 16; published 2023 March 20

Abstract

By studying the normalized cumulative radial distribution (nCRD) of the stars in the central region of a Monte Carlo-simulated globular cluster, we recently defined three parameters able to pinpoint the stage of internal dynamical evolution reached by the system: A_5 (i.e., the area subtended by the nCRD within 5% of the half-mass radius, r_h), P_5 (the value of the nCRD at 5% r_h), and $S_{2.5}$ (the slope of the nCRD at 2.5% r_h). Here we extend the analysis and explore the effects that different fractions (0%, 10%, and 20%) of primordial binaries and stellar mass black holes (BHs) induce on the dynamical history of the system. As expected, the gradual contraction of the cluster becomes milder and core collapse shallower for an increasing binary fraction. Nevertheless, the cluster dynamical evolution is still properly traced by the three parameters. For models with a larger initial retention of stellar mass BHs, the evolution depends on the timescale of their subsequent dynamical ejection. An early dynamical ejection of BHs results in a long-term evolution of the three parameters similar to that found in systems without initial BH retention. Conversely, in the model that retains a large number of BHs for an extended time (slow dynamical ejection of BHs), the system is characterized by a less concentrated structure and by the lack of significant temporal evolution of the three parameters. The lower values of the three parameters found in this case might be used to indirectly infer the possible presence of BHs in the cluster.

Unified Astronomy Thesaurus concepts: [Globular star clusters \(656\)](#); [Stellar dynamics \(1596\)](#)

1. Introduction

Globular clusters (GCs) are gas-free stellar systems that can harbor up to a few million stars of different masses. They are the most populous and oldest systems where stars can be individually observed. At odds with what happens in galaxies, where the orbital motion of stars primarily depends on the average gravitational potential, GCs are dynamically active (collisional) systems, where two-body interactions cause kinetic energy exchanges among stars and gravitational perturbations to their orbits, bringing the cluster toward a nearly thermodynamically relaxed state on a timescale (the relaxation time) that can be significantly shorter than their age. Because of these interactions, high-mass stars tend to progressively sink toward the central region of the cluster (dynamical friction), while low-mass stars preferentially escape from the system. This yields a progressive contraction of the core, producing a significant increase in its density: the so-called core collapse (CC). The runaway contraction is halted by the energy provided by the binary systems, and the post-CC phase is characterized by oscillations in the core size and central density. The recurrent gravitational interactions among stars thus progressively modify the structure of the system at a rate that depends in a very complex way on the initial and local conditions (e.g., the total cluster mass, the central density, the fraction of binaries and dark remnants, and the orbit within the host galaxy). Hence, in spite of a comparable chronological age, different clusters can have very different dynamical ages (e.g., Meylan & Heggie 1997). Determining the dynamical

evolutionary stage of star clusters is important not only for a complete physical understanding of these systems, but also because internal dynamic processes can have a significant impact on their stellar population and observational properties. For instance, blue straggler stars and millisecond pulsars are not predicted by the stellar evolution models of single objects, but they originate in dynamical processes involving direct stellar collisions and/or the evolution of binary systems (e.g., McCrea 1964; Hills & Day 1976; Bhattacharya & van den Heuvel 1991; Sills et al. 1997). Hence, their frequency and properties depend on the dynamical stage of the system and can be used to obtain information on the internal dynamics of GCs (see, e.g., Freire et al. 2004; Ransom et al. 2005; Ferraro et al. 2009, 2018, 2019; Verbunt & Freire 2014). In addition, other events such as neutron star and white dwarf mergers are thought to be enhanced in CC clusters, with important implications for our understanding not only of the internal dynamics of the system itself, but also, for example, of the rate of type Ia supernovae, and the origin of short gamma-ray bursts (see, e.g., Grindlay et al. 2006; Rodriguez et al. 2016; Kremer et al. 2021, see discussion in Ye et al. 2020). The approach most commonly adopted to estimate the dynamical ages of the clusters and to establish their current dynamical phase relies on the properties of the projected density profile of the system and its comparison with King (1966) models. The study of the cluster density profile may reveal features associated with, for example, the CC or the post-CC phase and allows the determination of the relaxation timescale for the inner regions of the cluster (e.g., Djorgovski & King 1984; Djorgovski 1993; Ferraro et al. 2003, 2009). These diagnostics, however, have been found to be not fully reliable and univocal in properly assessing the level of dynamical evolution reached by star clusters, and alternative indicators have been proposed in recent



Original content from this work may be used under the terms of the [Creative Commons Attribution 4.0 licence](#). Any further distribution of this work must maintain attribution to the author(s) and the title of the work, journal citation and DOI.

years, either based on peculiar populations of heavy stars (e.g., blue stragglers) that are sensitive tracers of the dynamical friction efficiency (e.g., Ferraro et al. 2012, 2018, 2019; Lanzoni et al. 2016), or based on the internal mass and kinematic structure of each system (e.g., Baumgardt & Makino 2003; Bianchini et al. 2016, 2018; Tiongco et al. 2016; Webb & Vesperini 2017; Bhavana Bhat et al. 2022, in preparation). In particular, in Bhavana Bhat et al. (2022, in preparation, hereafter, B22), we used a first set of Monte Carlo simulations following the evolution of a GC well beyond CC to define three new empirical parameters able to measure the dynamical age of the system from the normalized cumulative radial distribution (nCRD) of the stellar population in the central region of the cluster. Specifically, we observed that the shape of the nCRD progressively varies with time according to the system’s dynamical evolution, and we defined three parameters that appear to efficiently trace and quantify these morphological changes: they are called A_5 , P_5 , and $S_{2.5}$ (see Section 4.2). The investigation presented in B22 shows that these nCRD-based parameters progressively increase with time, reach their maximum values at CC, and then exhibit some oscillations during the post-CC phase, closely tracing the dynamical evolution of the system. Hence, they appear to be very promising empirical tools for assessing the dynamical evolutionary stage reached by star clusters. However, that first study explored a limited set of initial conditions not including primordial binaries or a significant fraction of dark remnants, such as black holes and/or neutron stars. These objects are observed in GCs (e.g., Milone et al. 2012; Sollima et al. 2012; Strader et al. 2012; Chomiuk et al. 2013; Giesers et al. 2018, 2019, and references therein) and are known to play a relevant role in the dynamics of stellar systems. In fact, the heating effect of these objects weakens (and then halts) the core contraction (see, e.g., Vesperini & Chernoff 1994; Trenti et al. 2007; Chatterjee et al. 2010), and they are also thought to substantially affect the structural properties of the host system (e.g., Sigurdsson & Phinney 1993; Mackey et al. 2007, 2008; Morscher et al. 2015), also quenching mass segregation (see, e.g., Gill et al. 2008; Alessandrini et al. 2016).

The present work is thus specifically aimed at quantifying the effect of primordial binaries and stellar mass black holes on the time evolution of the three parameters defined in B22. The paper is organized as follows. In Section 2 we describe the initial conditions of the Monte Carlo simulation runs and the method we adopted in the following analysis. In Section 3 we present the determination of the projected star density profile and the adopted King fit procedure. Section 4 describes the method and assumptions used for the construction of the nCRDs, and the definition and properties of the three nCRD dynamical indicators in the case of three different fractions of primordial binaries. In Section 5, nCRD parameters are compared with the expected values of the same parameters from the King model. Section 6 is devoted to the analysis of the effects induced by a subsystem of black holes. The summary and conclusions of the work are discussed in Section 7.

2. Methods and Initial Conditions

In this paper, we use five Monte Carlo simulations performed with the MOCCA code (Giersz et al. 2013; Hypki & Giersz 2013) to thoroughly follow the dynamical evolution of GCs with different primordial binary fractions and dark remnant retention fractions. In addition to two-body relaxation

Table 1
Initial Conditions of the Simulations

Name	W_0	BF	$r_h(\text{pc})$	$R_g(\text{kpc})$	other
BF0	6	0	2	4	...
BF10	6	10	2	4	...
BF20	6	20	2	4	...
DRr	6	0	2	4	Reduced kick velocity for black holes
DRe	7	10	1	2	Reduced kick velocity for black holes

Note. Values of the dimensionless central potential (W_0), binary fraction (BF), half-mass radius (r_h), and galactocentric distance (R_g) adopted as initial conditions in the five Monte Carlo simulations analyzed in this paper (see their names in the first column).

and tidal truncation effects, the code also models stellar and binary evolution by means of the codes SSE and BSE (Hurley et al. 2000, 2002), thus providing for each star at any evolutionary time not only the position and the velocity, but also the mass, and the B - and V -band magnitudes. One of the simulations is the same as presented in B22, and it is used here for comparison purposes. It initially has 500 K stars with masses ranging between 0.1 and $100M_\odot$, following a Kroupa (2001) mass function, and distributed as a King (1966) model with dimensionless central potential $W_0 = 6$. Supernova kicks are assumed to follow a Maxwellian distribution with a dispersion equal to 265 km s^{-1} (Hobbs et al. 2005). The cluster is tidally underfilling, with a three-dimensional half-mass radius $r_h = 2 \text{ pc}$ and a Jacobi radius equal to 61 pc (corresponding to the value that the system would initially have if it were orbiting at a galactocentric distance $R_g = 4 \text{ kpc}$). No primordial binaries are included in this run, which is referred to as BF0 throughout the paper. Two other simulations have been performed using the same initial conditions, except for their primordial binary fraction; these simulations start with a total number of single and binary stars, $N = N_s + N_b = 500 \text{ K}$ and a binary fraction $N_b/(N_s + N_b)$ equal to 10% and 20% in the runs that are referred to as BF10 and BF20, respectively. The distribution of binary properties (e.g., mass ratio, period, and eccentricity) are set according to the eigenevolution procedure described in Kroupa (1995) and Kroupa et al. (2013). The same initial conditions as those of the BF0 model, but with a reduced kick velocity for stellar black holes, were also used in the fourth simulation (which we call DRr). The fifth simulation, hereafter referred to as DRe, has slightly different initial conditions: the initial cluster density profile follows that of a King model with $W_0 = 7$, $r_h = 1 \text{ pc}$, and $R_g = 2 \text{ kpc}$. It starts with a 10% primordial binary fraction, and similar to the DRr run, it has a reduced kick velocity for the stellar mass black holes. With the DRr and DRe simulations, we explore the effect of dark remnants (retained black holes) on the cluster evolution and the time dependence of the three parameters introduced in B22. The initial conditions of all the simulations are listed in Table 1.

While the analysis of the DRr and DRe simulations is addressed separately in Section 6, Figure 1 shows the time evolution of the 1% Lagrangian radius ($r_{1\%}$, i.e., the radius including 1% of the total cluster mass) for the BF0, BF10, and BF20 runs. This clearly illustrates the evolution of the cluster’s inner structure and how it is affected by the presence of binary systems. In all cases, an initial expansion (driven by heavy

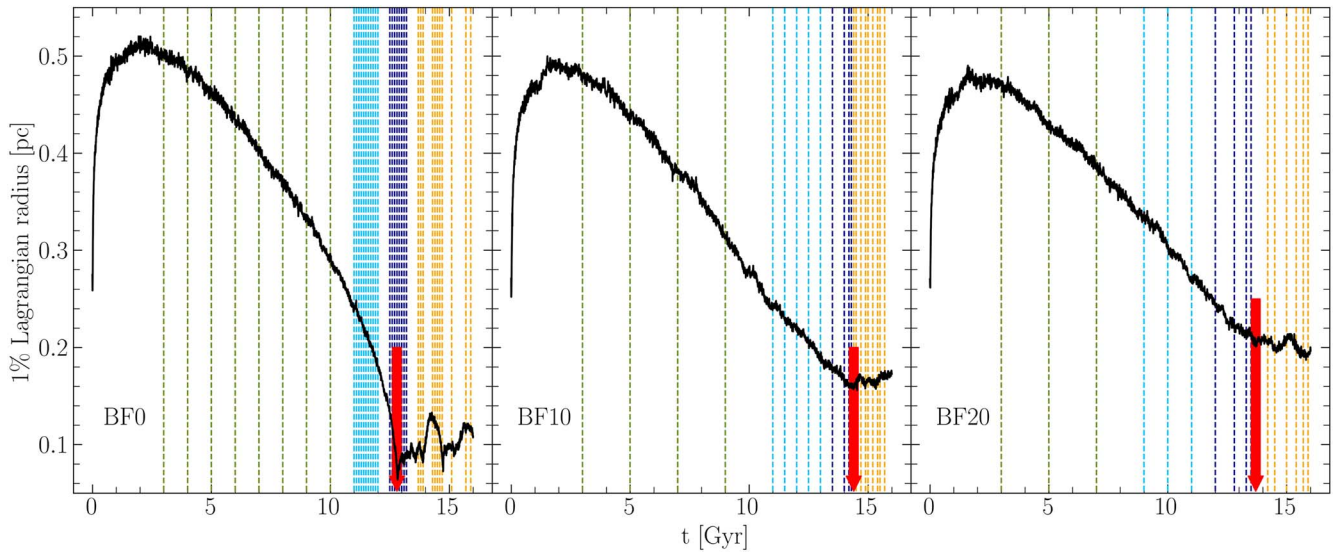


Figure 1. Time evolution of the 1% Lagrangian radius (black line) of the three simulations differing only in their primordial binary fraction: no primordial binaries in run BF0 (left panel), and 10% and 20% initial binary fractions in simulations BF10 and BF20 in the central and right panels, respectively. The vertical lines in each panel mark the time snapshots extracted and analyzed in each run, color-coded following the different evolutionary stages of the system: green, cyan, blue, and yellow for early, pre-CC, CC, and post-CC phases, respectively. The time of CC ($t_{CC} = 12.8, 14.4,$ and 13.7 Gyr for BF0, BF10, and BF20, respectively) is marked with a large red arrow in all the panels.

mass loss from young, massive stars) is followed by a phase in which two-body relaxation becomes dominant. This leads to a progressive contraction of the core, which culminates in the CC event when $r_{1\%}$ reaches the lowest value (red arrows in the figure). The CC time, t_{CC} , is approximately equal to $t_{CC} = 12.8$ Gyr, $t_{CC} = 14.4$ Gyr, and $t_{CC} = 13.7$ Gyr for the BF0, BF10, and BF20 simulations, respectively. As apparent and as expected, the overall effect of primordial binaries is to reduce the depth of CC and quench the post-CC gravothermal oscillations. In fact, if no primordial binaries are present, the system undergoes a phase of deep CC, until enough binaries are dynamically formed (see Giersz et al. 2013 and Giersz 2001 for details on the procedure for dynamical binary formation in MOCCA) in the core and stop the contraction. Conversely, in a cluster with substantial primordial binaries, the core contraction is hindered by binary burning (binaries acting as energy sources), which prevents the system from undergoing deep CC. Indeed, Figure 1 shows that the rapid phase of deep contraction immediately before CC is almost bypassed, and the CC event is reached in a smoother way in the BF10 and BF20 runs. While $r_{1\%}$ shrinks by a factor of 8 in the BF0 simulation, the factor is reduced to ~ 3 in the BF10 run and to 2.5 in the case of 20% primordial binaries. A clear phase of gravothermal oscillations, during which $r_{1\%}$ undergoes cyclic expansions and contractions, can clearly be distinguished after CC in the BF0 simulation, but it is absent in our simulations with primordial binaries.

To more quantitatively examine the impact of primordial binaries on the cluster dynamical evolution, in the following sections we extend the same analysis as was presented in B22 (for the BF0 run) to the BF10 and BF20 cases. Here we summarize the main aspects of the work, while more details about the adopted procedures can be found in the previous paper. As in B22, we extracted different time snapshots corresponding to various phases of the cluster dynamical evolution in the three runs. They are shown in Figure 1 with vertical dashed lines, color-coded as follows: green for the

early slow contraction phase, cyan for the subsequent phase leading to CC, blue for the CC phase, and yellow for the the post-CC phase. Following the approach adopted in B22, every snapshot is assumed to be a possible configuration of a real cluster observed in different stages of its dynamical evolution, and to be as consistent with real cases as possible, the simulated data were analyzed from the point of view of an observer. Thus, standard procedures and approximations adopted in observational works were applied: in each snapshot, the simulated cluster is projected onto a 2D plane, and a distance of 10 kpc from the observer was assumed to transform the distances from the center of the system from parsecs to arcseconds. In addition, binary systems were treated as stellar blends, consistently with the fact that the two components cannot be individually resolved at the distances of Galactic GCs. Hence, the magnitude of each binary system was determined by summing the luminosities of the two stellar components.

3. Projected Density Profiles

As part of the analysis, we first investigate the effect of different initial binary fractions on the development and evolution of an inner density cusp through various epochs of the cluster dynamical evolution. To construct the density profile of each extracted snapshot, we followed the same procedure as described in B22 and adopted in several observational works (e.g., Miocchi et al. 2013). It essentially consists of counting the number of stars in concentric annuli around the cluster center, and dividing it by the area of each radial bin. We then used a χ^2 method to determine the King (1966) model best-fitting the observed density profile by exploring a grid of models, with the dimensionless parameter W_0 (which is proportional to the gravitational potential at the center of the system) varying between 4 and 10.75 in steps of 0.05. This corresponds to a concentration parameter c spanning the interval between 0.84 and 2.5, with c being defined as the

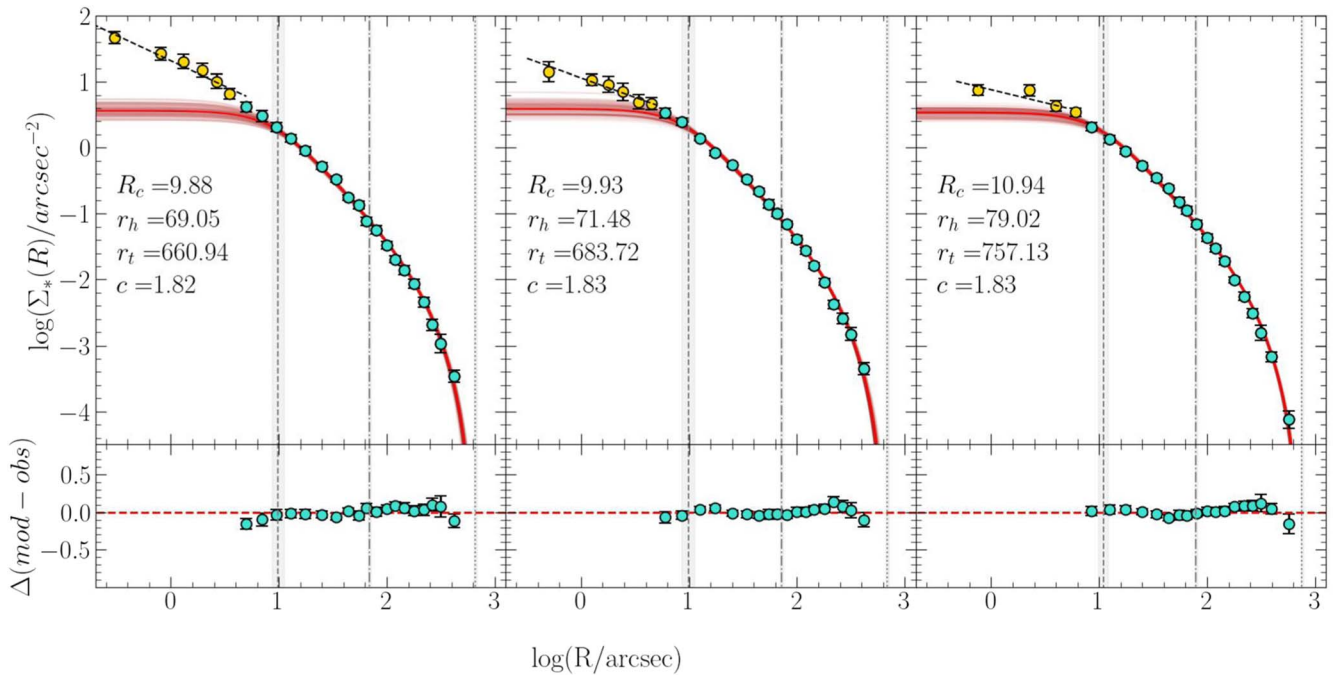


Figure 2. Projected density profile for the snapshots extracted at $t_{\text{CC}} = 12.8, 14.4,$ and 13.7 Gyr in the BF0 (left panel), BF10 (central), and BF20 (right) simulations, respectively. The solid red lines correspond to the King models that best fit the density profiles beyond $5''$ from the center (cyan circles), while the innermost cusps (yellow circles) are best fit by the dashed straight lines. The shaded red regions correspond to the uncertainty of the best-fit model. The vertical dashed, dot-dashed, and dotted lines indicate the core, half-mass, and truncation radii, respectively, calculated from the best-fit King models (see also the labels). The bottom panels show the residual between the best-fit model and the observed density profile.

logarithm of the ratio of the truncation or tidal radius of the system (r_t), and the King radius r_0 , which is the characteristic scale-length of the model: $c = \log(r_t/r_0)$. The King model profile describes the density distribution of the simulated clusters well, except for the snapshots close to and beyond CC, when a density cusp develops in the center. In these cases, the model still provides a very good fit to the external portion of the profile (cyan circles and red lines in Figure 2), while the trend in the innermost $\sim 5''$ is better fit with a power law (yellow circles and dashed lines in the figure). A density cusp always develops around the CC phase in all the simulations, and when it is formed, it never disappears. However, while it is prominent in the BF0 run, it becomes shallower and sometimes hardly distinguishable in the cases of 10% and, ever more so, 20% primordial binaries. Thus, the slope of the density cusp developed in the CC stage is affected by the binary content of the cluster, consistently with the effect discussed above on the time evolution of the 1% Lagrangian radius (Figure 1): star clusters with larger primordial binary fractions experience shallower CC and develop less steep cusps in the star density profile at the CC epoch (see also Vesperini & Trenti 2010).

While the King parameters obtained from the fit after the exclusion of the innermost $5''$ properly reproduce the external portion of the density profile, they cannot be used as an appropriate description of the overall cluster structure. In addition, the choice of $5''$ is somewhat arbitrary, and by changing this value, the resulting best-fit King model may change as well. To overcome these issues, we thus determined the King models that best fit the entire density profile of each snapshot, and we adopted the corresponding structural parameters in the following analysis (for more details, see Section 3.1 and Figure 2 in B22).

4. The nCRD Dynamical Indicators

Here we extend the analysis presented in B22 to the case of GCs including a population of primordial binary systems to test how the newly defined dynamical indicators, quantifying the morphology of the nCRD of cluster stars, depend on the primordial binary fraction. In the following, we therefore adopt the same method as was fully described in B22 and aim at making the three parameters well measurable from observations.

4.1. Normalized Cumulative Radial Distribution

For each extracted snapshot, we selected all the stars brighter than $V_{\text{cut}} = V_{\text{TO}} + 0.5$ (with V_{TO} being the V-band magnitude of the main-sequence turn-off point) to build the nCRD, and located within a projected distance equal to $0.5 \times r_h$ from the center. In the case of binary systems, we considered the combined magnitude of the two components because all binaries remain unresolved (they are observed as stellar blends) at the distance of GCs. These choices are motivated by the fact that the same procedure will be applied in future investigations to observational data, for which proper magnitude selections are needed to avoid problems of photometric incompleteness, and a common radial cut in units of a physical scale-length (as r_h) is required to allow a comparison among stellar systems of different intrinsic sizes. More specifically, we defined $x = R/r_h$ and considered all the magnitude-selected stars located between $x = 0$ and $x = 0.5$. For any value of x , the nCRD is equal to the number of stars within x and is normalized by the total number of selected stars. Hence, by construction, the nCRD is a curve that monotonically increases from 0 at the center ($x = 0$) to 1 at $x = 0.5$. The steeper this curve, the higher the concentration of the selected stars toward the center of the system.

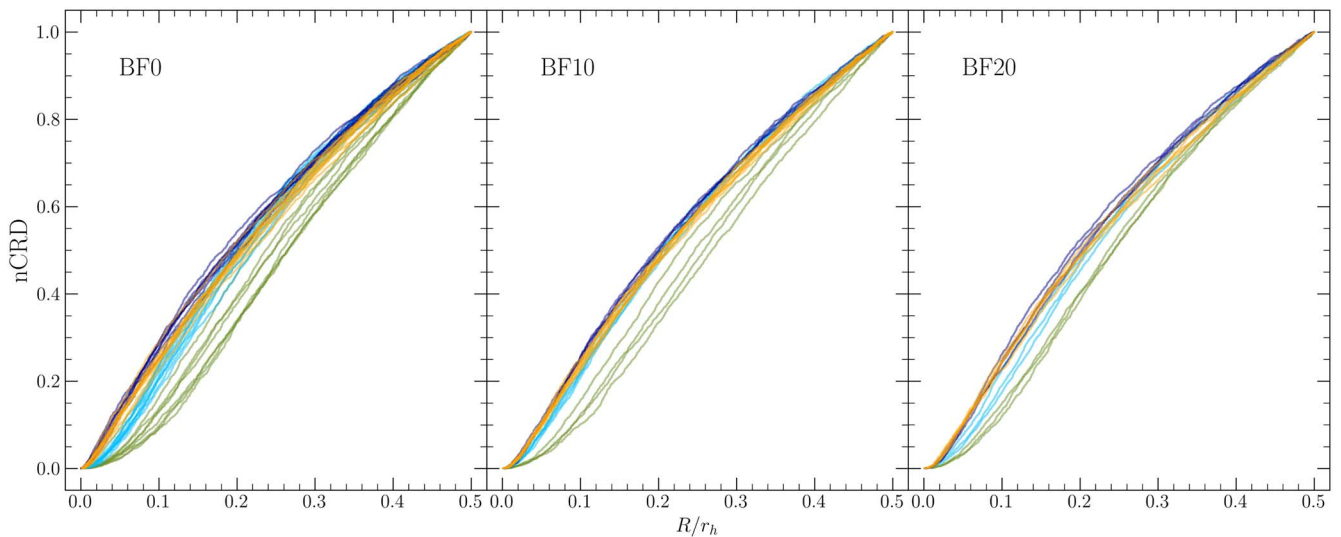


Figure 3. Normalized cumulative radial distributions of stars brighter than $V = V_{\text{TO}} + 0.5$ and located within $0.5 \times r_h$ from the center for all the snapshots analyzed in the BF0, BF10, and BF20 simulations (left, central, and right panels, respectively). The color-coding is the same as adopted in Figure 1: early times (green), pre-CC stages (cyan), CC phase (blue), and post-CC epoch (yellow).

Figure 3 shows the nCRDs thus obtained for all the snapshots extracted from the three simulations, color-coded as in Figure 1. Clearly, the morphology of the nCRDs changes with time following the cluster dynamical evolution, with shallower curves (less centrally segregated stars) for early evolutionary times (green lines), and increasingly steeper functions for more advanced dynamical stages. These morphological differences are stronger in the BF0 case and become progressively less pronounced in the BF10 and BF20 runs. This is another manifestation of the different depth of CC in the three cases (see Figure 1). In fact, in the absence of a primordial population, the binaries present in the cluster are limited to those dynamically generated in the core during the most advanced stages of evolution. Hence, they have little effect on the progressive segregation of cluster stars toward the center. Conversely, in a system with a substantial fraction of primordial binaries, binary burning provides the energy needed to halt core collapse earlier. Thus, the primordial binary fraction does affect the extent of morphological differences imprinted on the nCRD by the internal dynamical evolution of the system.

4.2. The A_5 , P_5 , and $S_{2.5}$ Parameters

In B22 we defined⁴ the following three parameters quantitatively describing the temporal variations of the nCRD caused by the cluster dynamical evolution:

1. A_5 is the area subtended by each nCRD between the center and a projected distance equal to 5% r_h (hence, between $x = 0$ and $x = 0.05$, with $x = R/r_h$);
2. P_5 is the value of the nCRD at 5% r_h ($x = 0.05$), which corresponds to the fraction of selected stars located within this distance from the center;

⁴ While the definitions of the three parameters are exactly the same as in B22, we emphasize that here, they are computed by using distances normalized to the half-mass radius $x = R/r_h$, while in B22, the adopted normalization was $0.5 \times r_h$. This has no impact on the results or the time evolution of the parameters; the only difference is that the values of A_5 plotted here are half of those published in B22, and those of $S_{2.5}$ are approximately twice the previous ones.

3. $S_{2.5}$ is the slope of the straight line tangent to the nCRD at 2.5% r_h (at $x = 0.025$). More specifically, it is the slope of the tangent to the third-order polynomial function that best fits the nCRD (the fit being introduced to smooth out the noisy behavior of the nCRD itself).

They are all defined in the very central region of the cluster to best sample the radial distance at which the dynamical effects that cause the central density growth during the core contraction and the CC phase are most relevant, and the nCRD morphological differences are maximized. The main source of error for the parameters is the uncertainty in the value of the half-mass radius derived from the King models. However, as discussed in B22, the size of these errors is negligible, and they are therefore ignored here.

By construction, these parameters quantify the evolution of the nCRD, and they increase as a function of the cluster dynamical age. This is clearly shown in Figure 4 (top, middle, and bottom panels for the A_5 , P_5 , and $S_{2.5}$ parameters, respectively). In the early dynamical phases (green symbols), each parameter shows a nearly constant behavior, taking essentially the same (low) values regardless of the primordial binary fraction. Then, they increase in the pre-CC phase (cyan symbols), reach a peak at the CC epoch (blue symbols), and show some fluctuations during the post-CC stage (yellow symbols), never receding to the initial low values. The gradual growth with time of the parameters is most pronounced in the BF0 simulation (left panels) and becomes milder for larger binary fractions (central and right panels). This is indeed expected for the same reasons as discussed above, reflecting the shallower CC and the lack of gravothermal oscillations in the models with 10% or 20% primordial binary fraction. Nevertheless, the clear increasing trend with time confirms the effectiveness of these parameters as proper tracers of the dynamical aging of the system.

For a deeper investigation of these dynamical indicators and to allow a direct comparison with observations, we removed the explicit dependence on time by plotting one parameter against another. The three possible combinations are shown in Figures 5, 6, and 7, where the dashed lines are the polynomial

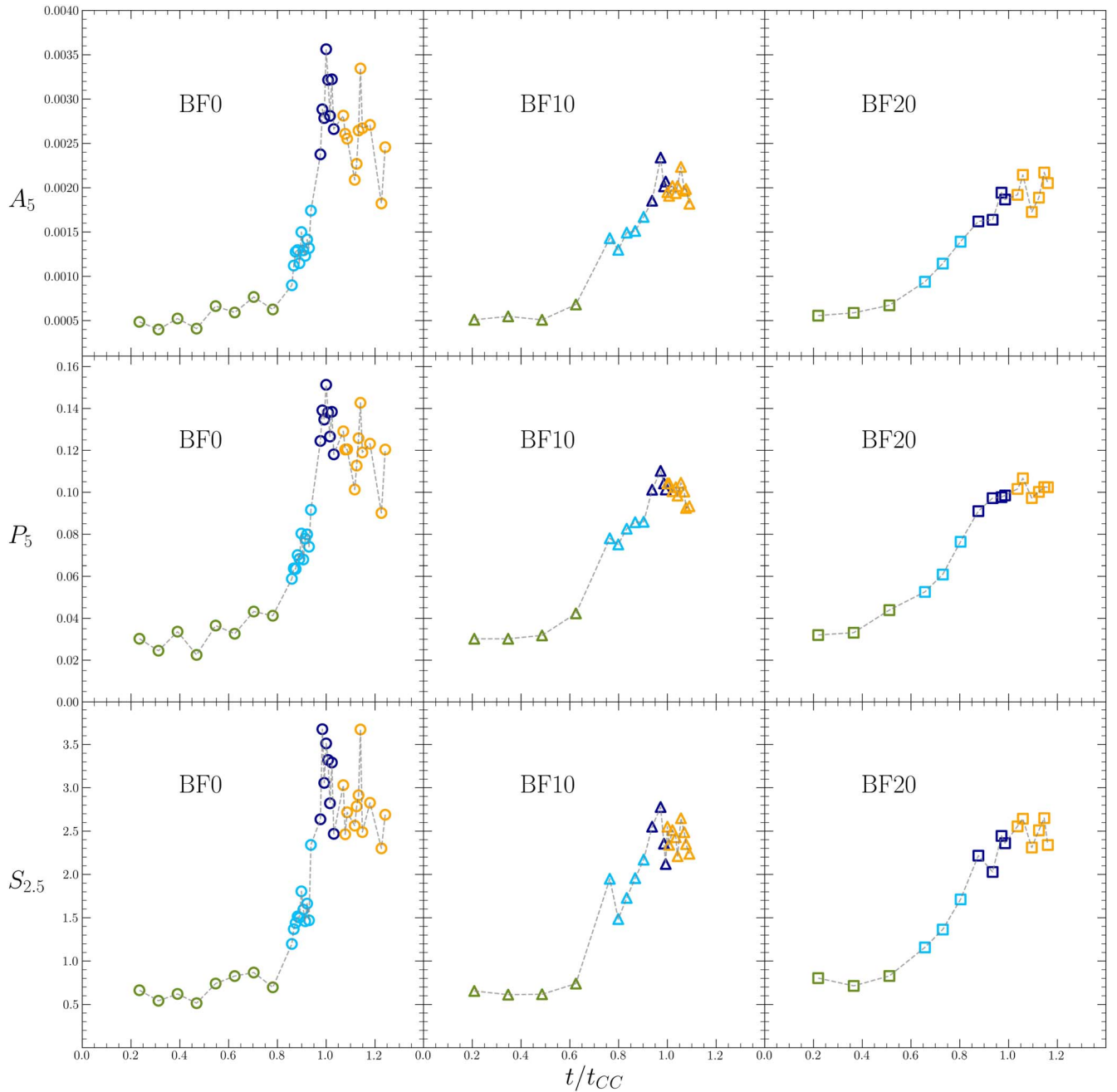


Figure 4. Time evolution of the A_5 , P_5 , and $S_{2.5}$ parameters (top, middle, and bottom panels, respectively) in the BF0, BF10, and BF20 simulations (left, central, and right panels, respectively). Time is normalized to the CC time of the corresponding simulation. The color-code is the same as in Figure 1.

fits to the distributions of points in the BF0 case (left panels), and they are reported for reference also for the BF10 and BF20 runs in the central and right panels, respectively. As shown by these figures, the measured values gradually move from the bottom left to the top right corner of each diagram for increasing dynamical age, up to CC (i.e., from green to cyan and then blue). Then, in the post-CC stage (yellow symbols) they tend to be lower than or mixed with those obtained during CC. The point distributions essentially follow the same relation (dashed lines in the figures) in all the simulations, regardless of the binary fraction. In principle, then, just from the measure of two parameters, these diagrams allow one to understand whether a stellar system is in an early, intermediate, or advanced stage of dynamical evolution, although the range of

values sampled by the parameters decreases for increasing binary fraction because the core contraction is weaker. This illustrates the complexity of univocally deriving the internal dynamical stage of the cluster if the primordial binary fraction is unknown. Nevertheless, these diagrams also show that some useful information can still be obtained. In fact, regardless of the binary fraction, the bottom left corner of these plots is exclusively populated by dynamically young systems (green symbols), and the highest values found for the BF20 run correspond to quite evolved systems in the other cases as well. In addition, if in an observed cluster values of A_5 , P_5 , and $S_{2.5}$ are measured that fall in the top right corner of these diagrams, a large binary content can be excluded, and the cluster is likely to be in a quite advanced stage of dynamical evolution.

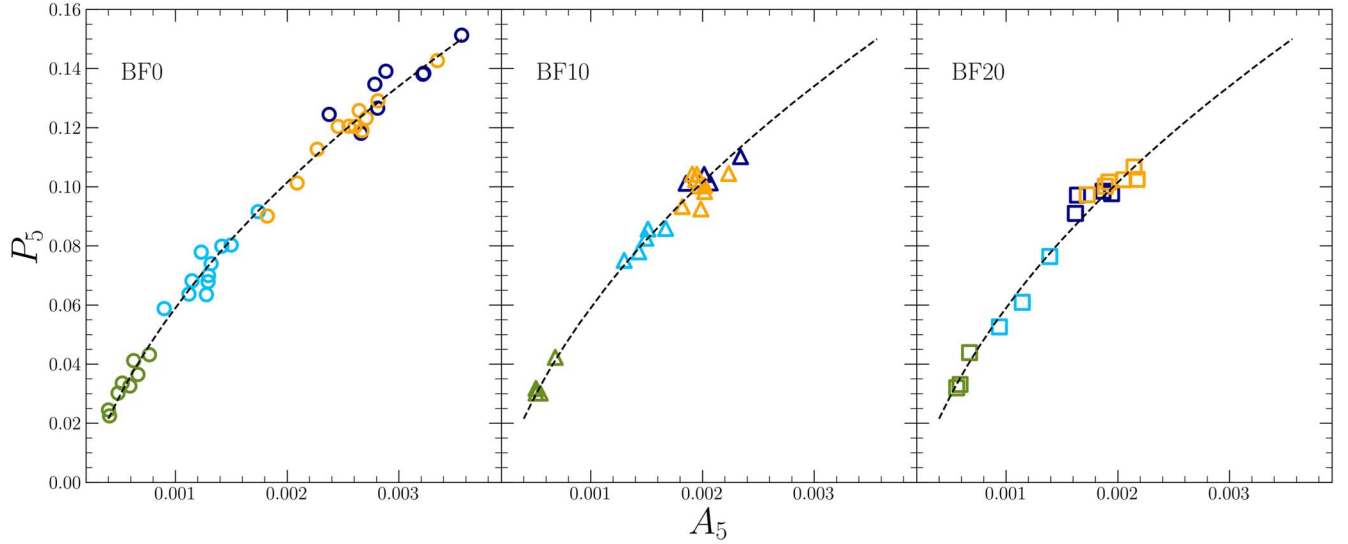


Figure 5. P_5 parameter plotted against A_5 for the BF0, BF10, and BF20 simulations (left, central, and right panels, respectively). The color-code is the same as in all previous figures. The dashed black lines are the polynomial fit to the distribution obtained in the BF0 run. It is reported for reference in the central and right panels as well.

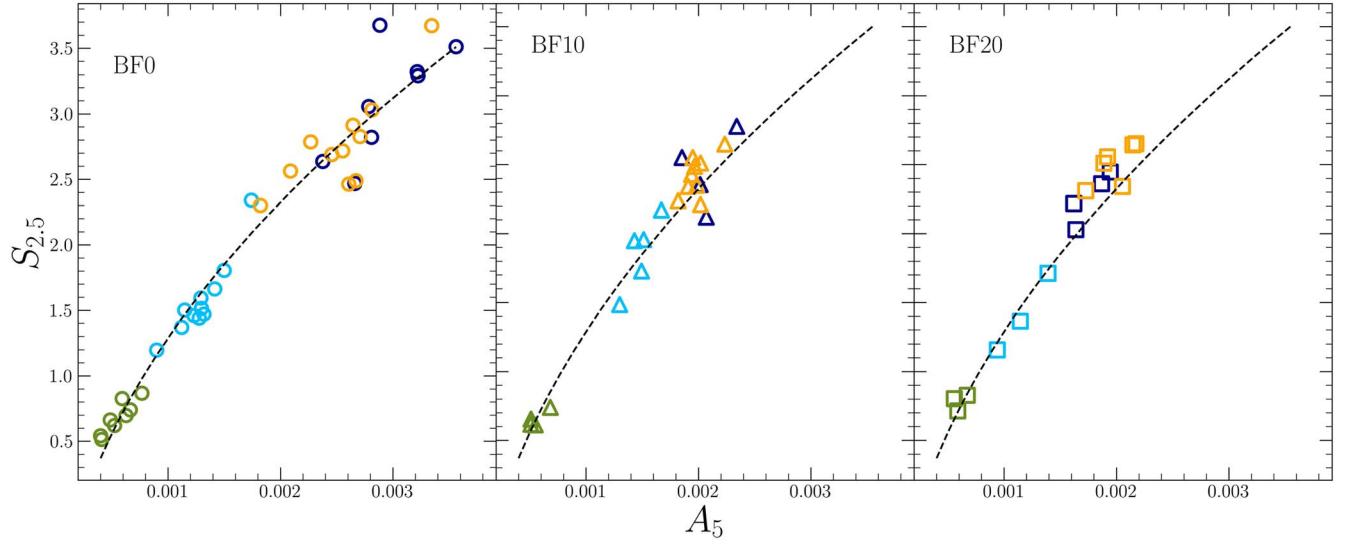


Figure 6. As in Figure 5, but for the $S_{2.5}$ parameter plotted against A_5 .

5. Zooming on the Deviations from King Models

By definition, the nCRD traces the projected radial distribution of stars with respect to the cluster center. Thus, it strictly depends on the projected density distribution of the system. In turn, the latter is commonly described through the King model family, which provides very good fits for clusters in early dynamical stages, but it shows significant discrepancies in the central regions for dynamically evolved systems (see Section 3 and, e.g., Figure 4 in B22). We therefore built the nCRDs by directly integrating the King model density profile for different values of the concentration parameter c between ~ 1 and 2.5, and we used these functions to measure the three dynamical indicators defined above. The results obtained for the A_5 parameter are shown in Figure 8 as empty black circles. The colored symbols in the figure correspond to the values determined from the actual nCRDs of the simulations, built as described in Section 4.2, plotted as a function of the concentration parameter of the King models that best fit the

observed density profiles for each extracted snapshot. The bottom panels show the relative difference between the parameter obtained from the actual nCRD and the parameters obtained from the King model integration: $\epsilon = (A_5 - A_5^{\text{King}})/A_5^{\text{King}}$. This figure shows that as expected from the gradual increase in the concentration of the system, the values of both A_5 and c increase from early (green) to intermediate (cyan) to evolved dynamical stages (blue and yellow). In addition, in the very early phases of dynamical evolution (green symbols), the density distribution is properly reproduced by the King family, and the A_5 parameter measured from the actual nCRDs is essentially the same as that obtained from the King models, regardless of the primordial binary fraction. Then, from the pre-CC stage (cyan) onward, the two measures of A_5 start to differ: in fact, the growth of the stellar density toward the center of the system makes the nCRDs increasingly steeper, and the value of A_5 starts to systematically and increasingly exceed the corresponding value of A_5^{King} . Hence, the A_5 parameter can be used as a sort of magnifier to

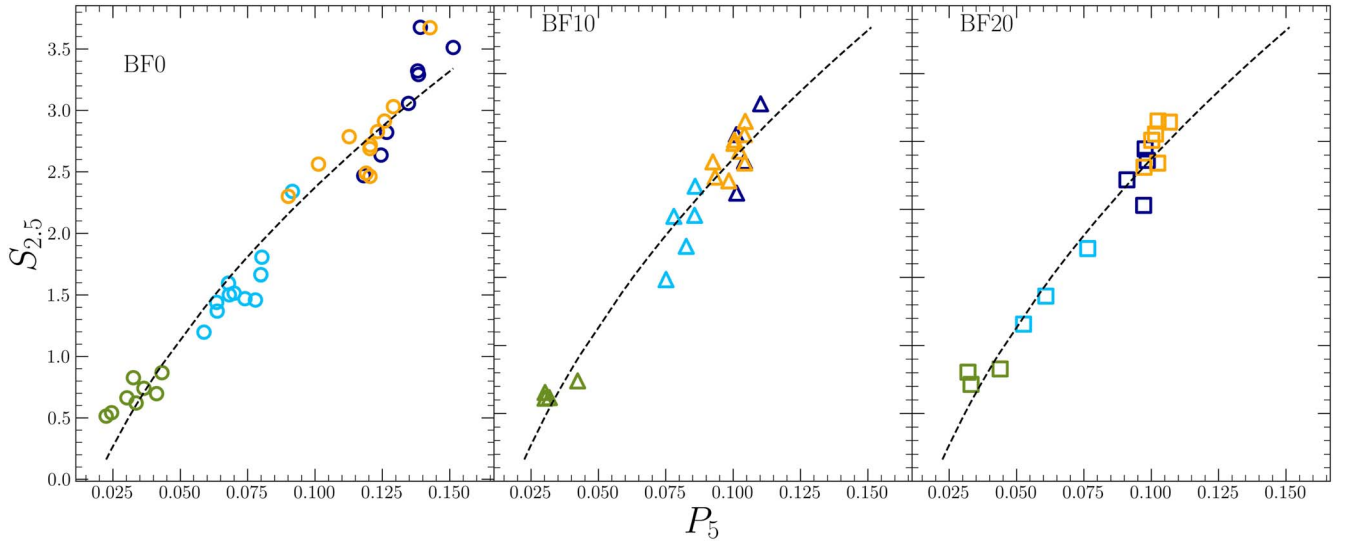


Figure 7. As in Figure 5, but for the $S_{2.5}$ parameter plotted against P_5 .

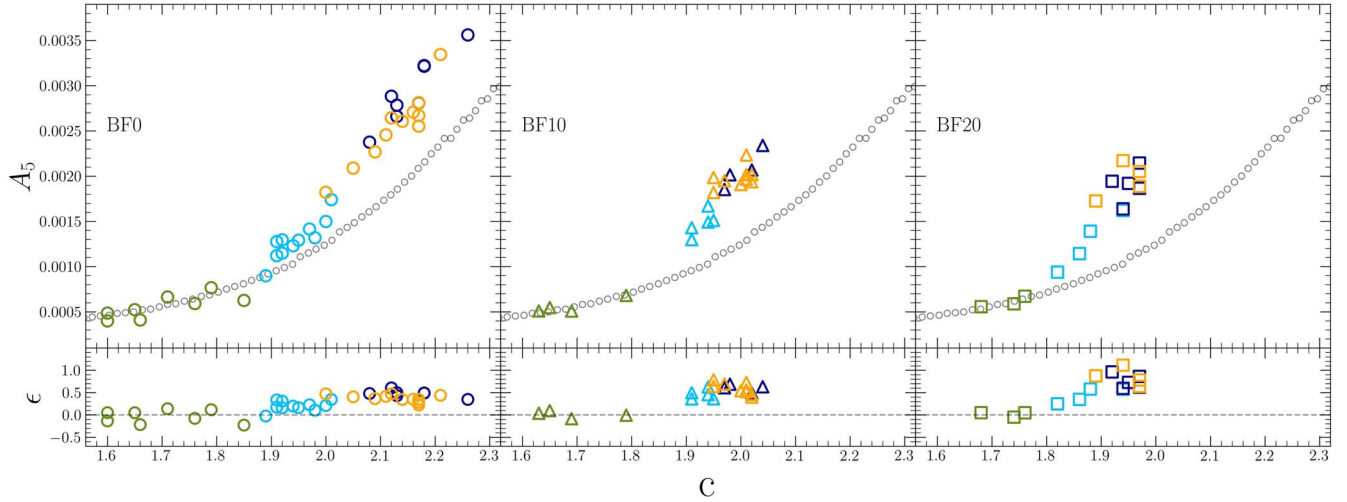


Figure 8. Values of A_5 measured from the direct integration of the King model density profile for different values of the concentration parameter c (empty black circles), compared to those obtained from the nCRDs of the extracted snapshots (colored symbols, the same as in the top row of Figure 4) plotted against the concentration parameter of the King models that best fit the density profile of each simulation. The left, central, and right panels refer to the BF0, BF10, and BF20 simulations, respectively. The bottom panels show the relative difference between the two measurements: $\epsilon = (A_5 - A_5^{\text{King}})/A_5^{\text{King}}$

pinpoint clusters whose density profile deviates from the King model distribution, well before the contraction of the system produces a measurable central cusp in the observed profile.

6. Effect of Dark Remnants on the nCRD Dynamical Indicators

While the previous sections focused on the effects of primordial binary systems, here we discuss how the nCRD dynamical indicators are affected by the presence of dark remnants. To this end, we consider the DRr and DRe simulations, where a reduced kick velocity for black holes is adopted according to the fallback prescription of Belczynski et al. (2002), thus significantly enhancing the fraction of black holes retained within the system potential well with respect to the BF0, BF10, and BF20 simulations. The time evolution of the number of black holes for the DRr and DRe runs is shown in Figure 9. As apparent, the ejection rate of black holes in the

DRe simulation (green circles) is much higher than that of the DRr simulation (indigo circles).

Figure 10 shows the time evolution of the 1% Lagrangian radius of the DRr and DRe runs (left and right panel, respectively). The extracted time snapshots are indicated by vertical dashed lines. At odds with the simulations discussed so far (compare to Figure 1), the evolution of $r_{1\%}$ in the DRr simulation shows an extended expansion phase lasting up to about 10 Gyr that is driven by the retained black holes. This long expansion phase is then followed by a gradual decrease in $r_{1\%}$, where two-body relaxation drives the cluster contraction. The system, however, never reaches the most advanced dynamical phases and the CC stage in a Hubble time. In the case of the DRe simulation (right panel of Figure 9), due to its higher ejection rate, most of the black holes are ejected by ~ 5 Gyr, and after that time, the inner regions of the cluster contract until the collapse is halted by primordial binaries at about 13.7 Gyr; the post-CC stages are similar to the BF10 and BF20 models.

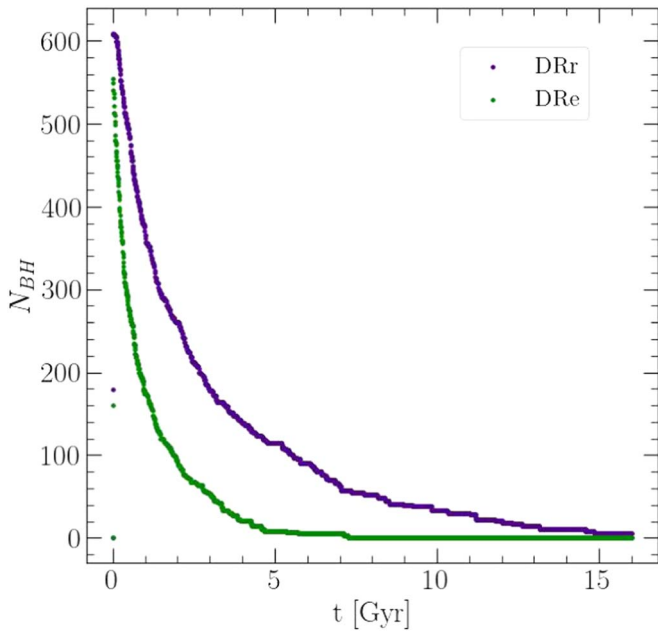


Figure 9. Time evolution of number of black holes in the two simulations with a large retention fraction of dark remnants: DRr (indigo circles) and DRe (green circles).

By adopting the same procedures as described in Section 4.1, we computed the nCRDs for all the extracted snapshots of DRr and DRe. The nCRDs for DRr are shown as indigo lines, and those of the DRe as green lines in the left and right panels of Figure 11, respectively. In the same figure, they are compared to the nCRDs obtained from the BF10 run (pink lines). At all evolutionary times, the nCRDs corresponding to the DRr run are all clumped (hence, they essentially show the same morphology) and have much shallower slopes than the BF10 run, implying a much smaller percentage of stars in the innermost regions as well, where the three dynamical indicators are defined. This is fully confirmed by the time dependence of A_5 , P_5 , and $S_{2.5}$ shown in Figure 12, where the values obtained from the DRr run (indigo diamonds) are compared to those measured in the BF10 and BF0 simulations (pink triangles and gold squares, respectively): the former always show much lower values than the others, and they are almost independent of time, which is consistent with the lack of a significant structural evolution displayed by $r_{1\%}$ in Figure 10. The shapes of the nCRDs of DRe evolve from having shallower slopes in the early snapshots (which are still affected by the expansion induced by the retained black holes) to having shapes indistinguishable from those of BF10 (at $t \geq 7$ Gyr, when essentially all the black holes have been ejected and the evolution becomes similar to that of BF10). Indeed, the time dependence of the dynamical indicators shown in Figure 12 for the DRe run (green circles) clearly starts from a low value similar to the DRr run and follows an increasing trend like in BF0 and BF10 runs. In particular, they are closer to the values of the BF10 run. This reflects the fact that even though the cluster starts with a significant number of dark remnants (hence the nCRDs are shallow and the dynamical indicators have low values, like in the DRr run), as the cluster loses all the black holes, it undergoes standard dynamical evolution, and the three dynamical indicators follow the trend of BF10 simulation, which has no dark remnants.

7. Discussion and Summary

In this paper, we have investigated the effects of different primordial binary fractions and dark remnant content on the value of three parameters that were specifically defined by B22 to quantify the dynamical evolution of the structural properties of star clusters. The (expected) impact of the fraction of binaries and dark remnants on the dynamical evolution of the system translates into a corresponding effect on the time dependence of the three parameters.

In the DRr run (where the rate of BH ejection is very low), the expansion effect due to the retained black hole system dominates most of the cluster’s dynamical evolution. As a consequence, no significant contraction of the cluster occurs (see the left panel of Figure 10), and the values of the three parameters remain essentially constant with time and are always much lower than those measured in all the other simulations (see Figure 12), where the number of black holes is below a few units either from the beginning (BF0, BF10, and BF20 runs) or for most of the cluster life (DRe simulation). Hence, although in this case, the nCRD parameters cannot help us in understanding the dynamical age of the cluster (also because it does not go across clearly distinct dynamical phases), measuring these low values might be used as an indication that the system still includes a significant number of stellar mass black holes (or, at least, that it retained a significant number of dark remnants for a large fraction of its life). The DRe run, which started with the same number of black holes as in the DRr simulation, but then ejected almost all of them during the initial ~ 5 Gyr of its evolution, essentially behaves as the models without dark remnant retention. This implies that while the three nCRD parameters cannot help us to distinguish among DRe and these latter cases, they allow us to determine the dynamical stage of star clusters with a high rate of black hole ejection, even if they initially retained a large number of these compact objects. However, deeper investigations are clearly needed, and this will be addressed in a forthcoming paper, where we will also investigate the impact of a central intermediate-mass black hole.

In the three models with different primordial binary fractions and no black hole retention, the general trend is that the values of the three parameters gradually increase with time and trace the internal dynamical evolution of the cluster. The time variations of A_5 , P_5 , and $S_{2.5}$ are most pronounced in the BF0 simulation, and they then become less marked in systems including primordial binary stars reflecting the milder contraction of these clusters. Strictly speaking, this implies that to properly infer the dynamical age of a cluster, one needs not only to measure the values of these parameters, but also to know the binary fraction of the system. Nevertheless, some general conclusions could be drawn even if this information were not available. In fact, Figures 4–7 show that low values of the three parameters ($A_5 \lesssim 0.0006$, $P_5 \lesssim 0.04$, and $S_{2.5} \lesssim 0.08$) indicate young dynamical ages, regardless of the binary content of the system. In addition, high values of the three parameters (as $A_5 \gtrsim 0.0023$, $P_5 \gtrsim 0.11$, and $S_{2.5} \gtrsim 2.7$) would univocally indicate a cluster in an advanced stage of dynamical evolution without or with very few primordial binaries. Indeed, the top right corner of these diagrams is always empty in the BF10 and BF20 simulations, and this can be used as indirect evidence against a large binary fraction in the system under analysis. Moreover, the comparison between the values of A_5 measured from the nCRD and those expected from the King model

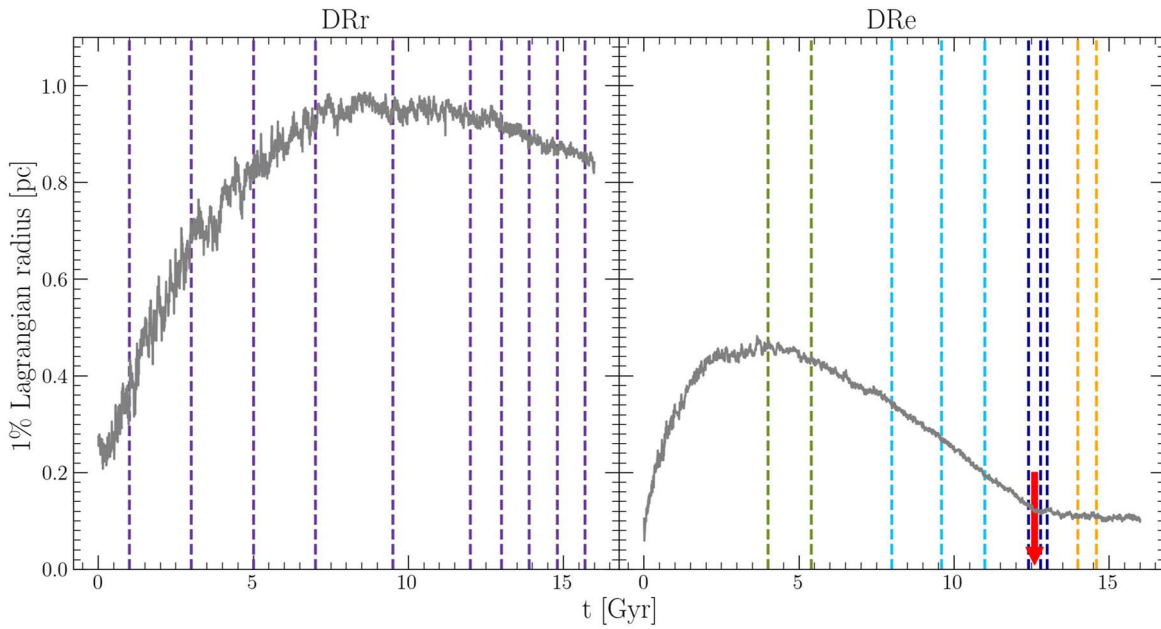


Figure 10. Time evolution of 1% Lagrangian radii in the two simulations with a large retention fraction of dark remnants, DRr and DRe runs are shown in the left and right panels, respectively. The vertical dashed lines in indigo indicate the 10 time snapshots extracted from the DRr simulation, and the vertical dashed lines with the standard color-code used in previous figures show the 10 time snapshots extracted from the DRe simulation.

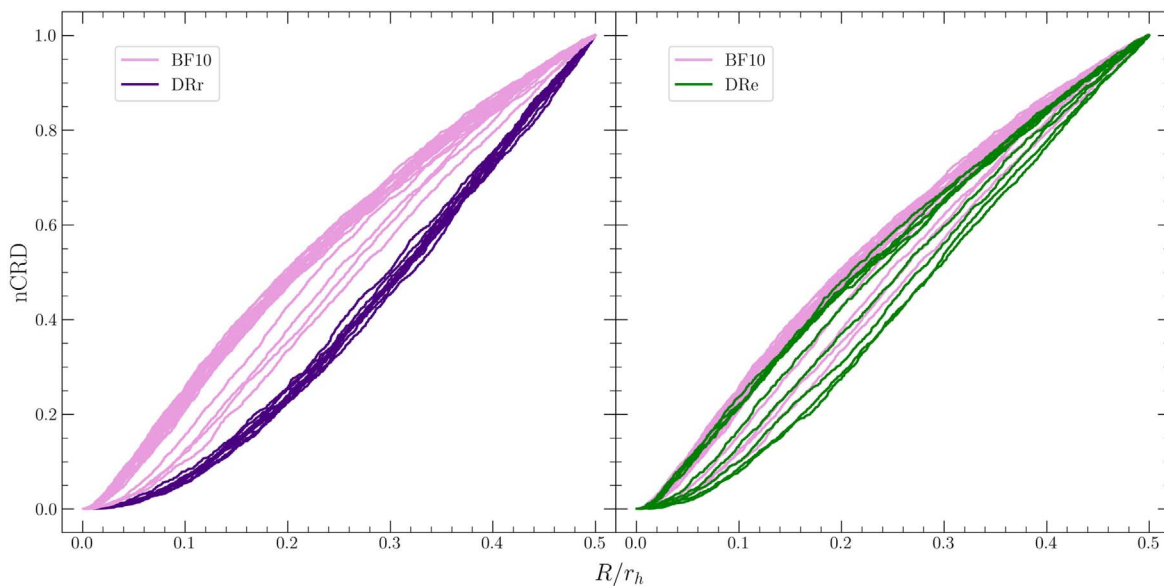


Figure 11. Normalized cumulative radial distributions for all the snapshots extracted from the DRr (indigo lines) and DRe (green lines) simulations in the left and right panels, respectively. They are compared to those obtained for the BF10 run (pink lines, same as in the right panel of Figure 3).

distribution (Figure 8) shows that this parameter is able to trace the progressive deviations from the King model expectations that occur during the late stages of dynamical evolution. Hence, in both theoretical and observational studies, A_5 can be used as a sort of magnifier to identify a dynamically old system well before its contraction produces a measurable central cusp in the density profile.

The analysis presented in this paper confirms that the three nCRD parameters introduced in B22 are very useful tools for investigating the dynamical stage of stellar systems, even in the cases of a nonzero primordial binary fraction and in the case of clusters with a high rate of black hole ejection. In this

investigation, the analyzed simulations follow the evolution of a given system over cosmic time, while the GCs in our galaxy all have essentially the same old age (~ 12 Gyr), but are observed in different stages of their internal dynamical evolution. A forthcoming paper (Bhavana Bhat et al. 2022, in preparation) will therefore be devoted to the analysis of the nCRD parameters in a sample of simulated clusters generated from a broad range of different initial conditions (hence, subject to different rates of internal dynamical evolution), but all considered at the same chronological age of ~ 12 Gyr. Meanwhile, we are also performing detailed measures of the nCRD parameters in real clusters, also discussing the

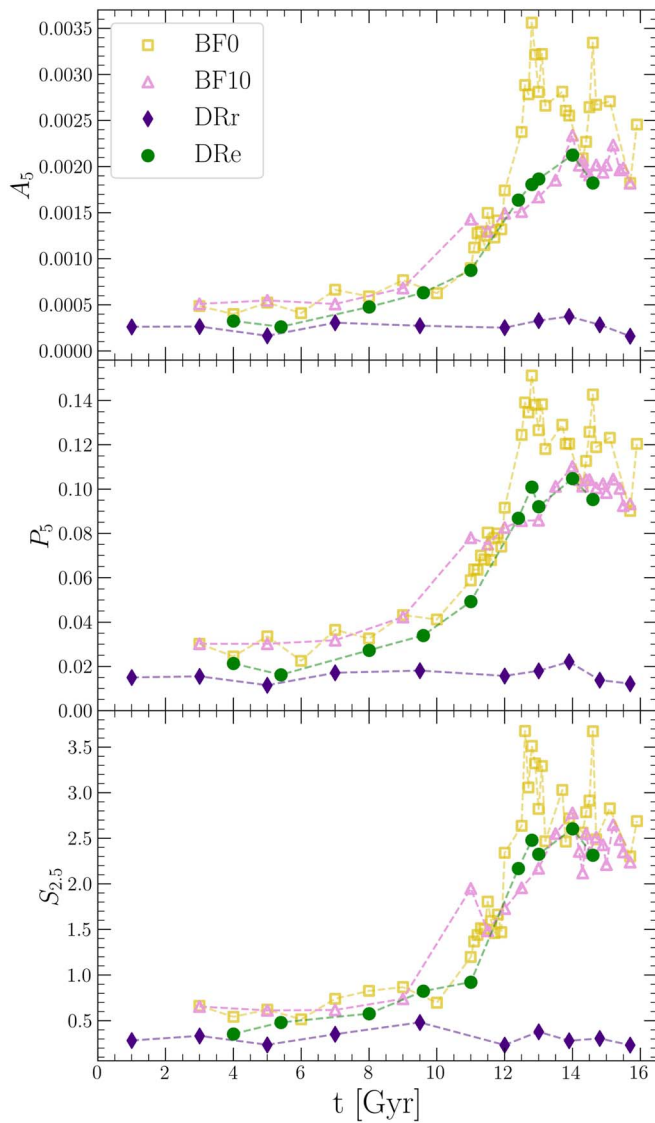


Figure 12. Time evolution of the A_5 , P_5 , and $S_{2.5}$ parameters for the DRr run (indigo diamonds) and the DRe run (green circles) compared to those measured in the BF10 and BF0 simulations (pink triangles and gold squares, respectively).

sensitivity of these new tools with respect to other dynamical indicators, in particular, the A^+ parameter measured from the blue straggler star population (see Ferraro et al. 2012, 2018, 2019, 2020; Alessandrini et al. 2016). This will finally provide a quantitative assessment of the operational ability of the three nCRD diagnostics to distinguish star systems in different stages of dynamical evolution.

This work is part of the project Cosmic-Lab at the Physics and Astronomy Department “A. Righi” of the Bologna University (<http://www.cosmic-lab.eu/Cosmic-Lab/Home.html>). The research was funded by the MIUR throughout the PRIN-2017 grant awarded to the project Light-on-Dark (PI: Ferraro) through contract PRIN-2017K7REXT.

ORCID iDs

B. Bhat <https://orcid.org/0000-0002-3578-6037>

B. Lanzoni <https://orcid.org/0000-0001-5613-4938>

F. R. Ferraro <https://orcid.org/0000-0002-2165-8528>

E. Vesperini <https://orcid.org/0000-0003-2742-6872>

References

- Alessandrini, E., Lanzoni, B., Ferraro, F. R., Miocchi, P., & Vesperini, E. 2016, *ApJ*, 833, 252
- Baumgardt, H., & Makino, J. 2003, *MNRAS*, 340, 227
- Belczynski, K., Kalogera, V., & Bulik, T. 2002, *ApJ*, 572, 407
- Bhattacharya, D., & van den Heuvel, E. P. J. 1991, *PhR*, 203, 1
- Bianchini, P., van de Ven, G., Norris, M. A., Schinnerer, E., & Varri, A. L. 2016, *MNRAS*, 458, 3644
- Bianchini, P., Webb, J. J., Sills, A., & Vesperini, E. 2018, *MNRAS*, 475, L96
- Chatterjee, S., Fregeau, J. M., Umbreit, S., & Rasio, F. A. 2010, *ApJ*, 719, 915
- Chomiuk, L., Strader, J., Maccarone, T. J., et al. 2013, *ApJ*, 777, 69
- Djorgovski, S. 1993, in ASP Conf. Ser. 50, Structure and Dynamics of Globular Clusters, ed. S. G. Djorgovski & G. Meylan (San Francisco, CA: ASP), 373
- Djorgovski, S., & King, I. R. 1984, *ApJL*, 277, L49
- Ferraro, F. R., Lanzoni, B., & Dalessandro, E. 2020, *Rendiconti Lincei. Scienze Fisiche e Naturali*, 31, 19
- Ferraro, F. R., Beccari, G., Dalessandro, E., et al. 2009, *Natur*, 462, 1028
- Ferraro, F. R., Lanzoni, B., Dalessandro, E., et al. 2012, *Natur*, 492, 393
- Ferraro, F. R., Lanzoni, B., Dalessandro, E., et al. 2019, *NatAs*, 3, 1149
- Ferraro, F. R., Lanzoni, B., Raso, S., et al. 2018, *ApJ*, 860, 36
- Ferraro, F. R., Possenti, A., Sabbi, E., et al. 2003, *ApJ*, 595, 179
- Freire, P. C., Gupta, Y., Ransom, S. M., & Ishwara-Chandra, C. H. 2004, *ApJL*, 606, L53
- Giersz, M. 2001, *MNRAS*, 324, 218
- Giersz, M., Heggie, D. C., Hurley, J. R., & Hypki, A. 2013, *MNRAS*, 431, 2184
- Giesers, B., Dreizler, S., Husser, T.-O., et al. 2018, *MNRAS*, 475, L15
- Giesers, B., Kamann, S., Dreizler, S., et al. 2019, *A&A*, 632, A3
- Gill, M., Trenti, M., Miller, M. C., et al. 2008, *ApJ*, 686, 303
- Grindlay, J., Portegies Zwart, S., & McMillan, S. 2006, *NatPh*, 2, 116
- Hills, J. G., & Day, C. A. 1976, *Astrophys. Lett.*, 17, 87
- Hobbs, G., Lorimer, D. R., Lyne, A. G., & Kramer, M. 2005, *MNRAS*, 360, 974
- Hurley, J. R., Pols, O. R., & Tout, C. A. 2000, *MNRAS*, 315, 543
- Hurley, J. R., Tout, C. A., & Pols, O. R. 2002, *MNRAS*, 329, 897
- Hypki, A., & Giersz, M. 2013, *MNRAS*, 429, 1221
- King, I. R. 1966, *AJ*, 71, 64
- Kremer, K., Rui, N. Z., Weatherford, N. C., et al. 2021, *ApJ*, 917, 28
- Kroupa, P. 1995, *MNRAS*, 277, 1491
- Kroupa, P. 2001, *MNRAS*, 322, 231
- Kroupa, P., Weidner, C., Pflamm-Altenburg, J., et al. 2013, in Planets, Stars and Stellar Systems: Galactic Structure and Stellar Populations, ed. T. D. Oswalt & G. Gilmore, Vol. 5 (Dordrecht: Springer Science +Business Media), 115
- Lanzoni, B., Ferraro, F. R., Alessandrini, E., et al. 2016, *ApJL*, 833, L29
- Mackey, A. D., Wilkinson, M. I., Davies, M. B., & Gilmore, G. F. 2007, *MNRAS*, 379, L40
- Mackey, A. D., Wilkinson, M. I., Davies, M. B., & Gilmore, G. F. 2008, *MNRAS*, 386, 65
- McCrea, W. H. 1964, *MNRAS*, 128, 147
- Meylan, G., & Heggie, D. C. 1997, *A&ARv*, 8, 1
- Milone, A. P., Piotto, G., Bedin, L. R., et al. 2012, *A&A*, 540, A16
- Miocchi, P., Lanzoni, B., Ferraro, F. R., et al. 2013, *ApJ*, 774, 151
- Morscher, M., Pattabiraman, B., Rodriguez, C., Rasio, F. A., & Umbreit, S. 2015, *ApJ*, 800, 9
- Ransom, S. M., Hessels, J. W. T., Stairs, I. H., et al. 2005, *Sci*, 307, 892
- Rodriguez, C. L., Chatterjee, S., & Rasio, F. A. 2016, *PhRvD*, 93, 084029
- Sigurdsson, S., & Phinney, E. S. 1993, *ApJ*, 415, 631
- Sills, A., Lombardi, J. C. J., Bailyn, C. D., et al. 1997, *ApJ*, 487, 290
- Sollima, A., Bellazzini, M., & Lee, J. W. 2012, *ApJ*, 755, 156
- Strader, J., Chomiuk, L., Maccarone, T. J., Miller-Jones, J. C. A., & Seth, A. C. 2012, *Natur*, 490, 71
- Tiongco, M. A., Vesperini, E., & Varri, A. L. 2016, *MNRAS*, 461, 402
- Trenti, M., Heggie, D. C., & Hut, P. 2007, *MNRAS*, 374, 344
- Verbunt, F., & Freire, P. C. C. 2014, *A&A*, 561, A11
- Vesperini, E., & Chernoff, D. F. 1994, *ApJ*, 431, 231
- Vesperini, E., & Trenti, M. 2010, *ApJL*, 720, L179
- Webb, J. J., & Vesperini, E. 2017, *MNRAS*, 464, 1977
- Ye, C. S., Fong, W.-f., Kremer, K., et al. 2020, *ApJL*, 888, L10